J. Plasma Phys. (2016), *vol.* 82, 905820205 © Cambridge University Press 2016
doi:10.1017/S0022377816000180

Relativistic thermal electron scale instabilities in sheared flow plasma

Evan D. Miller[1],† **and Barrett N. Rogers**[1]

[1]Department of Physics and Astronomy, Dartmouth College, Hanover, NH 03755, USA

(Received 29 September 2015; revised 1 February 2016; accepted 3 February 2016)

The linear dispersion relation obeyed by finite-temperature, non-magnetized, relativistic two-fluid plasmas is presented, in the special case of a discontinuous bulk velocity profile and parallel wave vectors. It is found that such flows become universally unstable at the collisionless electron skin-depth scale. Further analyses are performed in the limits of either free-streaming ions or ultra-hot plasmas. In these limits, the system is highly unstable in the parameter regimes associated with either the electron scale Kelvin–Helmholtz instability (ESKHI) or the relativistic electron scale sheared flow instability (RESI) recently highlighted by Gruzinov. Coupling between these modes provides further instability throughout the remaining parameter space, provided both shear flow and temperature are finite. An explicit parameter space bound on the highly unstable region is found.

1. Introduction

In recent years, researchers have identified numerous electron scale plasma instabilities (Weibel 1959; Bret, Firpo & Deutsch 2004; Gruzinov 2008; Alves *et al.* 2015) that are thought to be important in astrophysical and laboratory phenomena (Fiuza *et al.* 2012; Stockem *et al.* 2014), including shocks (Gregori *et al.* 2012), particle acceleration (Gruzinov & Waxman 1999; Medvedev & Loeb 1999) and magnetogenesis (Kulsrud & Zweibel 2008; Alves *et al.* 2012; Grismayer *et al.* 2013; Nishikawa *et al.* 2013; Alves *et al.* 2014; Miller & Rogers 2015). The electron scale Kelvin–Helmholtz instability (ESKHI) is one example. Classically, the KHI is a neutral fluid phenomenon driven by velocity shear (Biskamp 2003). The mode in its simplest form requires subsonic bulk velocity, and is strongest for wave vectors $k \sim 1/L$ parallel to the flow, where L is a typical gradient scale length of the flow profile. The ESKHI, which occurs in plasmas with sharp (electron scale) flow variations, is a related electromagnetic mode at higher frequencies and smaller scales (i.e. scale sizes comparable to the electron skin depth $d_e \equiv c/\omega_{pe}$). Recently, Gruzinov (2008) demonstrated that in the relativistic regime, there exists a second mechanism for shear-driven instability. This instability is electromagnetic, and operates at wavelengths longer than d_e, albeit with low growth rates when the shear velocity V_0 is small compared to the speed of light c. Very recently, Alves *et al.* (2012, 2015), Grismayer *et al.* (2013) have explored similar instabilities with wave vectors transverse

† Email address for correspondence: evanmiller124@gmail.com

https://doi.org/10.1017/S0022377816000180 Published online by Cambridge University Press

to the flow. The bulk of this previous work has assumed a cold plasma, $T_i = T_e = 0$. In the typical Kelvin–Helmholtz (KH) case of waves propagating parallel to the flow, we expand this effort to include finite temperatures, utilizing the relativistic fluid framework of Synge (1957, equations (B1)); this permits relativistically high temperatures (T_i, $T_e > m_i c^2$, $m_e c^2$). We find that quite generally, the addition of finite temperature is destabilizing. This is demonstrated for two simple cases; free-streaming ions (i.e. $V_i = V_0$ or equivalently $m_i \to \infty$) and equal thermal speeds ($V_{ti} = V_{te}$, relevant to the ultra-hot case or the case of electron–positron plasmas). With either constraint, unstable, purely growing modes (i.e. positive real roots to the dispersion relation) occur in two neighbouring parameter regimes, associated with Gruzinov's instability and the ESKHI. Outside these regions, the coupling of the modes produces residual instability; all wavenumbers in this domain are unstable, with maximum growth rates occurring for wavelengths near the electron skin depth ($k^{-1} \approx d_e$). Consequently, the system is unstable for any finite temperature. Because we utilize a fluid model, the applicability of this theory to collisionless plasmas is problem dependant. In such a system, these results should be interpreted with caution. That said, most of the existing studies on this topic use a kinetic approach (Bret *et al.* 2004; Alves *et al.* 2012, 2015; Grismayer *et al.* 2013); here we present a fluid treatment, which derives many of the same results.

Before continuing, we must clarify an ambiguity in the terminology. Two completely distinct effects are commonly referred to as the Kelvin–Helmholtz instability (KHI). Traditionally, the KHI is an acoustic phenomenon found in neutral fluids. This is the instability presented in most introductory texts (Biskamp 2003). It requires subsonic sheared velocity ($V_0 < V_t$) to operate, often implicitly assumed by using the incompressible equations. Gruzinov (2008) and Alves *et al.* (2015), on the other hand, use an electromagnetic analogue to the KHI. Gruzinov calls this effect (Gruzinov 2008) the 'relativistic collisionless Kelvin–Helmholtz instability'. Alves *et al.* (2015) refer to it as the electron scale Kelvin–Helmholtz instability (ESKHI). However, as both Alves *et al.* and Gruzinov assume $T = 0$ (or at least $V_t \ll V_0$), the physics of the effects they describe are fundamentally distinct from traditional KHI dynamics. Henceforth, we refer to their mode as the 'relativistic electron scale shear instability' (RESI). The term ESKHI is reserved for the electron scale, sub-thermal speed mode that was absent in Gruzinov's $T = 0$ work, i.e. the dispersion relation that, in the subsonic, non-relativistic, neutral limit, recovers the traditional KHI dispersion relation found in introductory texts (Biskamp 2003). Finally, note that the dynamics of both modes are distinct from effects arising in the context of standard electron magnetohydrodynamics with motionless ions, including the instability frequently referred to as the electron Kelvin–Helmholtz instability.

2. Description of instabilities

Consider a collisionless ion–electron plasma with discontinuous sheared flow in the centre-of-momentum frame (figure 1). The bulk velocity of ions and electrons is $V_0 \hat{\boldsymbol{y}}$ above the discontinuity and $-V_0 \hat{\boldsymbol{y}}$ below (these regimes are indicated by subscripts a and b where appropriate). Following Gruzinov (2008), we are analysing waves propagating in the y-direction, parallel to the flow. The unperturbed plasma is assumed to be unmagnetized, charge neutral and current free, with uniform density and pressures.

Assuming free-streaming ions ($m_i = \infty$) linear perturbations with wavenumber k along the discontinuity and growth rate λ satisfy a dispersion relation in terms

https://doi.org/10.1017/S0022377816000180 Published online by Cambridge University Press

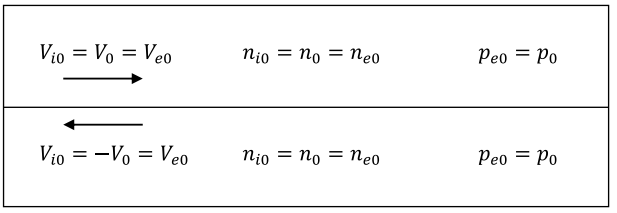


FIGURE 1. The Kelvin–Helmholtz shear discontinuity system.

of electron plasma frequency ω_e and thermal speed V_{te} (see appendix A for a discussion of the relativistic parameters). Normalizing velocities to the speed of light c, frequencies to the electron plasma frequency over the Lorentz factor $\gamma_0 = (1 - V_0^2)^{-1/2}$ and wavenumbers to the skin depth over γ_0 (B 10*a–d*), this dispersion relation is (a derivation of (2.1) is outlined in appendix B. A far more general equation including three dimensions and ion motion can be found in the supplementary materials available online at http://dx.doi.org/10.1017/S0022377816000180. This general equation encompasses the RESI, ESKHI and transverse mushroom instability found by Alves *et al.* (2015))

$$0 = S(\lambda) \equiv RFG - 2V_0^2 V_{te} \lambda^2 D^2, \tag{2.1}$$

where

$$F \equiv (\lambda^2 + V_0^2 k^2)^2 + \lambda^2 - V_0^2 k^2, \tag{2.2a}$$

$$D \equiv 1 + 2k^2 + \lambda^2 - V_0^2 k^2, \tag{2.2b}$$

$$G \equiv (1 + (\lambda - \mathrm{i}kV_0)^2) W_a + (1 + (\lambda + \mathrm{i}kV_0)^2) W_b, \tag{2.2c}$$

$$R \equiv \sqrt{1 + \frac{k^2}{\gamma_0^2} + \frac{\lambda^2}{\gamma_0^2}}, \tag{2.2d}$$

$$\text{and} \quad W_{a/b} \equiv \sqrt{1 + (\lambda \pm \mathrm{i}kV_0)^2 - (\pm \lambda V_0 + \mathrm{i}k)^2 V_{te}^2}. \tag{2.2e}$$

Assuming equal thermal speeds ($V_{ti} = V_{te}$) instead of free-streaming ions leads to an identical equation (upon substituting $\omega_p^2 = \omega_e^2 + \omega_i^2$ for ω_e^2); this is relevant to the ultra-hot limit, since as $T \to \infty$ thermal velocities cannot exceed $c/\sqrt{3}$ (see appendix A), or to an electron–positron plasma (assuming $T_e = T_p$). As shown in appendix B, W and R are the inverse decay lengths of the acoustic and light wave modes, respectively. The dispersion relation $F = 0$ is the RESI, with solutions (Gruzinov 2008):

$$\lambda^2 = \tfrac{1}{2}\left(-1 - 2V_0^2 k^2 \pm \sqrt{1 + 8V_0^2 k^2}\right). \tag{2.3}$$

$R = 0$ gives a plasma light wave with frequency $\lambda^2 = -k^2 - \gamma_0^2$, and $G = 0$ results in the electron acoustic mode/ESKHI, with roots given by a subset of

$$\lambda^2 = 0_+, \quad \frac{1}{1 + V_{te}^2 - 2V_0^2 V_{te}^2}\left(-1 - k^2 V_0^2 - V_{te}^2\left(\frac{k^2}{\gamma_0^4} - V_0^2 + 1 - k^2 V_0^2\right)\right.$$
$$\left. \pm \sqrt{4k^2 V_0^2 + 4k^2 V_0^2\left(\frac{k^2}{\gamma_0^4} - V_0^2\right) V_{te}^2 + \left(\frac{k^2}{\gamma_0^4} - V_0^2\right)^2 V_{te}^4}\right). \tag{2.4}$$

https://doi.org/10.1017/S0022377816000180 Published online by Cambridge University Press

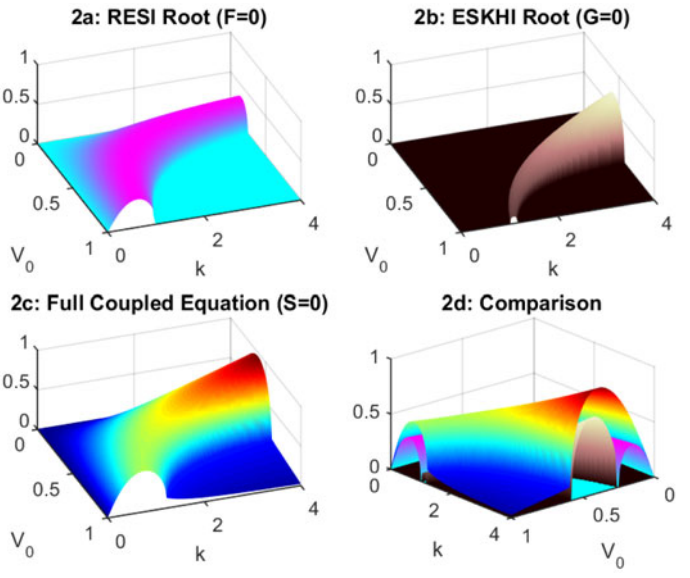


FIGURE 2. The growth rate of the most unstable roots as a function of V_0 and k, at $V_{te} = 0.4$.

For these three fundamental modes, the roots are either purely real (growing/decaying) or purely imaginary (oscillatory). It is straightforward to derive their regimes of instability; the RESI has unstable solutions in the range $0 < k^2 V_0^2 < 1$ (Gruzinov 2008) and the ESKHI is unstable when

$$1 < k^2 V_0^2 < 1 + V_{te}^2 k^2 \frac{2}{(1 + V_{te}^2)}. \tag{2.5}$$

The light wave mode is always stable. The second term in (2.1) provides a coupling between these modes. This coupling amplifies the existing purely real instabilities, while generating smaller, complex instabilities in previously stable parameter regimes.

Figure 2 highlights the relationships between roots of $F = 0$, $G = 0$ and $S = 0$. The surfaces show the maximum real part of λ, as a function of bulk velocity V_0 and wavenumber k, at a thermal speed $V_{te} = 0.4$. Figures 2(a) and 2(b) present the real portions of (2.3) and (2.4), respectively. The unstable regions of both functions are bounded by limits given above, meeting as predicted where $kV_0 = 1$. Outside of these boundaries, growth rates are purely imaginary. Figure 2(c) shows the real components of numerical roots for (2.1) at the same temperature. The coupling increases the growth rate of existing instabilities and merges the regimes of figures 2(a) and 2(b). Between the ESKHI cutoff (2.5) and $kV_0 = 0$, modes have highly unstable, purely real roots. In the region beyond this cutoff, residual coupling of the instabilities creates smaller, complex roots. In figure 2(d), the previous three plots are superimposed. This more clearly demonstrates that regions unstable to RESI or ESKHI independently are even less stable in the fully coupled equation. Furthermore, outside these bounds, lingering instability remains. Figure 3 presents numerical solution to (2.1) at various temperatures. As temperature increases, instability (in normalized units) increases everywhere. The regime of large instability also stretches along both axes, as suggested by (2.5).

https://doi.org/10.1017/S0022377816000180 Published online by Cambridge University Press

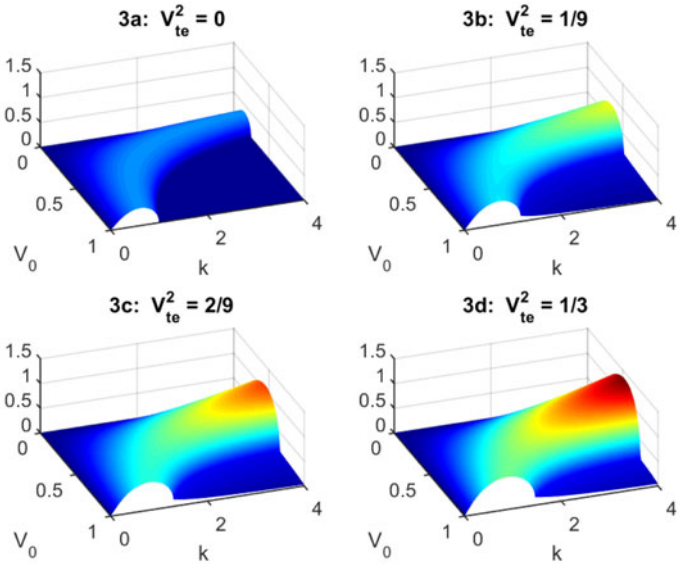


FIGURE 3. The growth rate of the most unstable roots of equation (2.1) ($S = 0$) as a function of V_0 and k for various V_{te}.

Before discussing the complex roots in depth, we prove that the highly unstable roots are purely real, and that the bound on the region of high instability closely matches the bound on ESKHI given in (2.5). The function $S(\lambda)$ is holomorphic everywhere that $Re(\lambda) \neq 0$ (a sufficient but not necessary condition). Thus for all non-zero real λ, $S(\lambda)$ is real. As λ goes to real infinity, $S(\lambda)$ grows to positive infinity as well (the leading term proportional to λ^8 is positive). Therefore, if $S(\lambda)$ is negative for small λ, there must exist some positive real value which satisfies $S(\lambda) = 0$, i.e. there must exist a purely growing unstable mode. Taylor expanding (2.1), a positive real root is guaranteed when

$$k^2 V_0^2 \leqslant 1 + V_{te}^2 k^2 \frac{2}{(1 + V_{te}^2)}. \tag{2.6}$$

Thus the upper bound on the domain of real roots for ESKHI (2.5) is also a sufficient condition for a real root to the fully coupled equation $S(\lambda)$. Numerical modelling shows that this closely matches the necessary condition as well; only in a narrow parameter regime is $S(\lambda)$ positive for $\lambda \ll 1$ and negative at some finite λ (thus generating a pair of roots; these narrow regions appear in figures 4 and 5). It can also be noted that there is exactly one positive real root when (2.6) is met, and that when $k^2 V_0^2 < 1 + V_{te}^2 k^2$ the root at $\lambda = 0_+$ vanishes as well.

Figures 4 and 5 illustrate the progression of the roots of $S(\lambda)$ as V_{te} increases. Both figures plot the absolute value of the function $S(\lambda_{real} + i\lambda_{imag}, V_{te})$, for $V_0^2 = 1/2$, $k = 2$. Thus, roots exist where the surfaces hit zero (deep blue). Note that to remove spurious roots, the actual function being plotted is $S/(((\lambda + ikV_0)^2 + 1)((\lambda - ikV_0)^2 + 1))$. Figure 4 shows the λ_{real}–λ_{imag} plane, at various V_{te} slices (while only the fourth quadrant is presented, $S(\lambda)$ is symmetric across both axes). A video version of this

https://doi.org/10.1017/S0022377816000180 Published online by Cambridge University Press

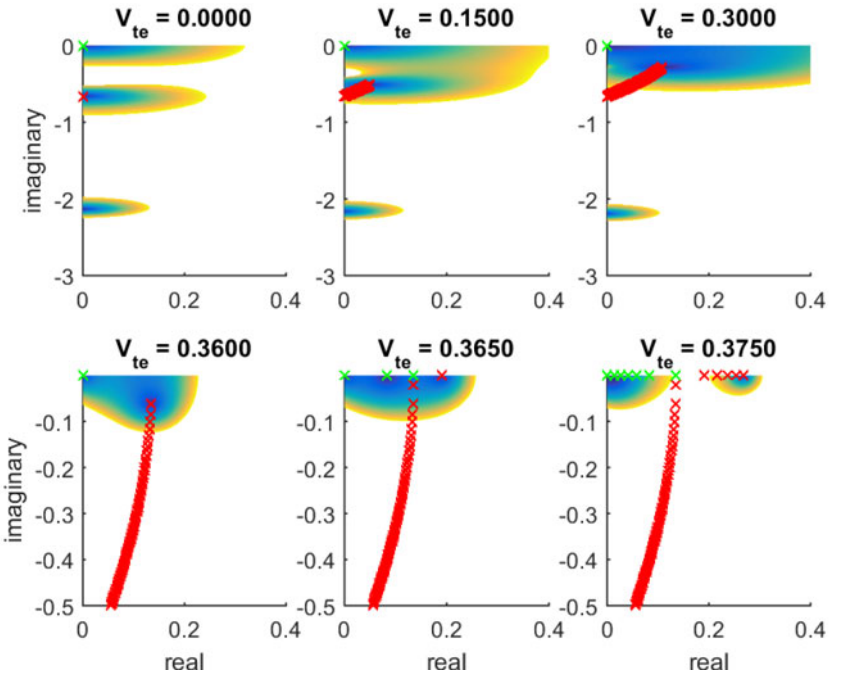


FIGURE 4. The absolute value of $S(\lambda_{real} + \mathrm{i}\lambda_{imag})$, using $V_0^2 = 1/2$, $k = 2$, and increasing values of V_{te} '×' marks indicate the path of the roots as V_{te} increases from zero in steps of $\Delta V_{te} = 0.0025$ For the top three images, the colour scales go from 0 (blue) to 3 (red). In the bottom three, the max cutoff is 0.1. Videos of this motion are available online.

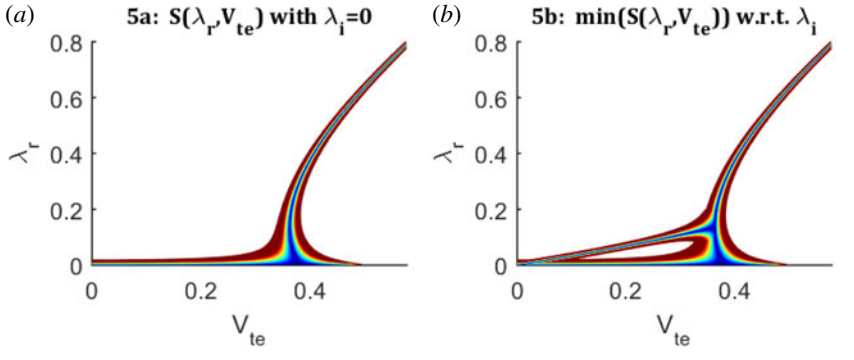


FIGURE 5. The absolute value of $S(\lambda_{real}, V_{te})$, using $V_0^2 = 1/2$, $k = 2$. (*a*) assumes $\lambda_{imag} = 0$. In (*b*), the minimum of $S(\lambda_{real}, V_{te})$ with respect to λ_{imag} is presented.

figure, which is perhaps more illuminating, can be found in the supplementary movie online. At $V_{te} = 0$, the roots are the purely imaginary solutions to $R = 0$, $F = 0$ and $G = 0$. Once finite temperature is included, the coupling term in (2.1) interferes. The positive RESI root (tracked by red '×' marks) drifts off the imaginary axis. The ESKHI root at $\lambda = 0_+$ remains (green ×), but the negative RESI root ceases to be a true zero of the equation, as does the light wave root. As V_{te} increases, the real

https://doi.org/10.1017/S0022377816000180 Published online by Cambridge University Press

component of what used to be the positive RESI root continues to increase and the imaginary component decreases. Isolating the thermal velocity in (2.6) results in

$$V_{te}^2 < \frac{k^2 V_0^2 - 1}{1 + 2k^2 - k^2 V_0^2}. \tag{2.7}$$

Just prior to exceeding this condition, the root becomes purely real. The two roots on either side of the real axis merge and redivide into two roots along the real axis. One of these roots drops towards zero (marked in green), and the other increase rapidly with V_{te}. When the two sides of (2.7) are exactly equal, the falling root reaches zero and merges with the $\lambda = 0_+$ root ($\lambda = 0$ itself is not a root unless very specific parameters are chosen). For temperatures higher than this, there is only a single positive real root to the equation. Finally, when $k^2 V_{te}^2 = k^2 V_0^2 - 1$, $\lambda = 0_+$ ceases to be a root as well. Figure 5 shows the same behaviour from the λ_{real}–V_{te} plane. In figure 5(*a*), λ_{imag} is set to zero. In figure 5(*b*), the value plotted is the minimum of $S(\lambda_{real}, V_{te})$ across all λ_{imag}. The behaviour matches the above description. For low V_{te}, only complex roots and the root at $\lambda = 0_+$ exist. The instability grows with V_{te}, and just before the threshold of (2.7) is reached, the roots become purely real. There are briefly two positive real roots, one growing with V_{te} and one shrinking, the latter reaching zero when (2.7) is satisfied.

Before concluding, we will briefly comment on the connection between this work and the paper recently published by Alves *et al.* (2015). It is verified that for high V_0 and low V_{te}, there exists a k which maximizes growth rate (seen in (2.6) and figure 3). However, setting k to infinity in (2.6) results in the condition

$$V_0^2 \leqslant V_{te}^2 \frac{2}{(1 + V_{te}^2)}. \tag{2.8}$$

If (2.8) is satisfied, the system remains highly unstable for all wavenumbers and the growth rate increases as k goes to infinity. In the ultra-hot case $V_{te}^2 \to 1/3$, (2.8) reads $V_0^2 \leqslant 1/2$. Of course, this is assuming a discontinuity in the velocity profile; given a smoother shear with gradient scale length L, a maximizing wavelength will likely be found with $k \sim L^{-1}$ (Grismayer *et al.* 2013; Alves *et al.* 2014).

We also confirm the 'mushroom' instability described by Alves *et al.* (2015). Considering the transverse x–z plane instead of the parallel x–y plane, the dispersion relation

$$0 = (\lambda^2(\lambda^2 + 1) + k_z^2(\lambda^2 - \gamma_0^2 V_0^2)) \left(- \left(\frac{\lambda^2}{\gamma_0^2} + 1 \right) W' + V_0^2 V_t R' \right) \tag{2.9}$$

is reached (see the general 3-D equation presented in the supplementary material), where

$$W' = \sqrt{(\lambda^2 + 1) - \left(\lambda^2 V_0^2 - \frac{1}{\gamma_0^2} k_z^2 \right) V_{te}^2}, \quad R' = \sqrt{\frac{\lambda^2}{\gamma_0^2} + \frac{k_z^2}{\gamma_0^2} + 1}. \tag{2.10a,b}$$

The roots arising from the first factor are equivalent to (2.1) in Alves *et al.* (2015). The roots arising from the second factor are stable for all values of V_0, k_z and V_{te}. In general, parallel modes grow faster in the highly unstable regimes discussed above, and perpendicular modes grow more rapidly elsewhere. This connection demonstrates that in the discontinuity regime under consideration, the simple fluid model presented here derives the same results as the kinetic approach established by other researchers.

https://doi.org/10.1017/S0022377816000180 Published online by Cambridge University Press

3. Conclusion

We have shown that upon including temperature, parallel wave perturbations to relativistic shear flows are ubiquitously unstable at small scales. Strong instability (growth rates of order ω_p) occur in both the relativistic regime highlighted by Gruzinov (2008) and the standard ESKHI region; with free-flowing ions (or equal ion and electron thermal speeds), the condition for large instability is expressed in (2.6),

$$k^2 V_0^2 \leqslant 1 + V_{te}^2 k^2 \frac{2}{(1+V_{te}^2)}. \tag{3.1}$$

When this condition is met, we have found that growth rates are substantially larger in warm plasmas than in the $T=0$ plasmas studied previously (Weibel 1959; Gruzinov 2008; Alves *et al.* 2012, 2015) (up to triple for large temperatures); this parallels the findings of Grismayer's kinetic simulations (Grismayer *et al.* 2013). Even when velocity exceeds condition (3.1), a smaller, complex instability remains. In order to eliminate instability completely, it is necessary to eliminate the coupling term in (2.1). This requires setting either $V_0=0$ (i.e. no shear) or $T=0$ (cold plasma). As demonstrated in appendix B, the coupling term arises from the electromagnetic response to electron acoustic motion. When (2.8) is met, the growth rate appears to increase indefinitely with wavenumber. Otherwise, a fastest growing mode exists with wavelength near the electron skin depth. In a more physical scenario with smoother velocity gradient, presumably as in similar systems, the maximum growth rate is limited by the scale size of the shear (Grismayer *et al.* 2013; Alves *et al.* 2014). Finally, it is unlikely that the saturation condition of these modes will be substantially different than for the cold plasmas already studied. These instabilities saturate when the DC magnetic field they generate grows strong enough to arrest the flow of electrons across the field. Grismayer *et al.* estimate that this occurs around (Grismayer *et al.* 2013)

$$B = \frac{m_e \omega_e}{q} V_0 \sqrt{\gamma}_0. \tag{3.2}$$

For magnetogenesis applications, it is the growth of this field itself which is most important.

Supplementary material

Supplementary material is available at http://dx.doi.org/10.1017/S0022377816000180.

Appendix A. A note on relativistic variables

The relativistic analogues of the electron plasma frequency and electron thermal speed satisfy

$$\omega_e^2 \equiv \frac{q^2 n_0}{\varepsilon_0 m_e f_e \gamma_0^2}, \qquad \frac{V_{te}^2}{c^2} = \frac{\dfrac{z_e}{f_e}\dfrac{\mathrm{d}f_e}{\mathrm{d}z_e}}{z_e^2 \dfrac{\mathrm{d}f_e}{\mathrm{d}z_e} + 1}, \quad \text{where } z_e = \frac{m_e c^2}{T_e},\ f_e = \frac{K_3(z_e)}{K_2(z_e)}. \tag{A 1a,b}$$

The factor f_e, a ratio of two modified Bessel functions of the second kind, is the relativistic correction to mass due to thermal motion (similar to the Lorentz correction

https://doi.org/10.1017/S0022377816000180 Published online by Cambridge University Press

γ for linear motion). For a detailed analysis of this term and derivation of the thermal velocity, see Synge (1957). Importantly, for low temperatures, the classical result $V_t^2 = 5T/3m$ is recovered, while at high temperatures, a maximum V_t is reached,

$$\lim_{T\to\infty} \frac{V_t^2}{c^2} = \frac{1}{3}. \tag{A 2}$$

This is analogous to how the Lorentz factor γ prevents a particle's linear velocity from exceeding c, regardless of how much kinetic energy it possesses.

Appendix B. Derivation of instability

Following the work of Synge (1957) and Mahajan (2003), the equations for a relativistic plasma are found by integrating Vlasov equation assuming a Maxwell–Juttner distribution. They consist of species-specific continuity equations

$$\partial_\mu n_o U^\mu = 0, \tag{B 1a}$$

species-specific equations of motion

$$-\partial^\nu (n_o T) + m n_o U^\mu \partial_\mu (f U^\nu) = q n_o U_\mu F^{\nu\mu}, \tag{B 1b}$$

and the Maxwell equations

$$\partial_\nu F^{\mu\nu} = J^\mu \tag{B 1c}$$

$$\text{and } \varepsilon^{\alpha\beta\gamma\delta}\partial_\gamma F_{\alpha\beta} = 0, \tag{B 1d}$$

$$\text{with } J^\mu = \sum_s q_s n_o U_s^\mu, \tag{B 1e}$$

where n_o is the rest frame density, T is temperature, f is the Synge factor discussed in appendix A, m and q are particle mass and charge, U^μ is the four velocity, $F^{\mu\nu}$ is the electromagnetic tensor, ∂_ν is the four gradient and $\varepsilon^{\alpha\beta\gamma\delta}$ is the Levi-Civita symbol. Note that we employ the Einstein summation convention, and that the time component ($\nu = 0$) of the equation of motion gives an equation for pressure evolution (in lieu of an equation of state). In terms of the usual three-vector quantities, these become

$$\partial_t \boldsymbol{E} = c^2 \nabla \times \boldsymbol{B} - \frac{1}{\varepsilon_0}\boldsymbol{J}, \tag{B 2a}$$

$$\partial_t \boldsymbol{B} = -\nabla \times \boldsymbol{E}, \tag{B 2b}$$

$$\partial_t n = -\nabla \cdot (n\boldsymbol{V}), \tag{B 2c}$$

$$\left(1 - \frac{V_t^2 V^2}{c^4}\right)\partial_t p = -\left(1 - \frac{V_t^2}{c^2}\right)\boldsymbol{V}\cdot\nabla p - \frac{mfV_t^2 n}{\gamma}\nabla\cdot\boldsymbol{V} - \frac{V_t^2}{c^2}\frac{q_s n}{\gamma^2}\boldsymbol{V}\cdot\boldsymbol{E}, \tag{B 2d}$$

$$\text{and} \quad \partial_t \boldsymbol{V} = -\boldsymbol{V}\cdot\nabla\boldsymbol{V} + \frac{q_s}{mf\gamma}\left(\boldsymbol{E} - \frac{\boldsymbol{V}\boldsymbol{V}}{c^2}\cdot\boldsymbol{E} + \boldsymbol{V}\times\boldsymbol{B}\right) - \frac{\frac{\boldsymbol{V}}{c^2}\partial_t + \nabla}{n\gamma mf}p, \tag{B 2e}$$

where n is the lab frame density, c is the speed of light, $\gamma \equiv (1 - V^2/c^2)^{-0.5}$ is the Lorentz factor, V_t is the thermal speed discussed in appendix A and ε_0 is the permittivity of free space.

https://doi.org/10.1017/S0022377816000180 Published online by Cambridge University Press

Consider a plasma with unperturbed bulk velocity given by the Heaviside function $\boldsymbol{V}_0(\boldsymbol{x}) = V_0(2H(x)-1)\hat{\boldsymbol{y}}$ (figure 1). With free-streaming ions, assume perturbations to this flow proportional to $\mathrm{e}^{\lambda t+\mathrm{i}ky}$. Perturbations to electric field $\boldsymbol{E}$, magnetic field $\boldsymbol{B}$, electron velocity $\boldsymbol{V}_e$, electron density n_e and electron pressure p_e are thus

$$\boldsymbol{E}(\boldsymbol{x}) = (E_x(x), E_y(x), 0)\mathrm{e}^{\lambda t+\mathrm{i}ky}, \tag{B 3a}$$

$$\boldsymbol{B}(\boldsymbol{x}) = (0, 0, B(x))\mathrm{e}^{\lambda t+\mathrm{i}ky}, \tag{B 3b}$$

$$\boldsymbol{V}_e(\boldsymbol{x}) = (V_x(x), V_y(x), 0)\mathrm{e}^{\lambda t+\mathrm{i}ky}, \tag{B 3c}$$

$$n_e(\boldsymbol{x}) = n(x)\mathrm{e}^{\lambda t+\mathrm{i}ky}, \tag{B 3d}$$

$$\text{and } p_e(\boldsymbol{x}) = p(x)\mathrm{e}^{\lambda t+\mathrm{i}ky}. \tag{B 3e}$$

Linearizing the relativistic fluid (B 2), simple substitutions derive

$$\left(1+\frac{\omega_e^2}{\chi^2}\right)E_y - \frac{c^2}{(\lambda^2+c^2k^2+\omega_e^2)}\left(\left(1+\frac{\omega_e^2}{\chi^2}\right)E_y'\right)' = -\frac{\xi}{\chi^2}P + \frac{c^2}{(\lambda^2+c^2k^2+\omega_e^2)}\left(\frac{\xi}{\chi^2}P'\right)' \tag{B 4a}$$

$$\left(\frac{1}{V_{te}^2}-\frac{\xi^2}{\chi^2}\right)P - \frac{\lambda^2+c^2k^2}{(\lambda^2+c^2k^2+\omega_e^2)}\left(\frac{P'}{\chi^2}\right)' = \omega_e^2\left(\frac{\xi}{\chi^2}E_y - \frac{c^2}{(\lambda^2+c^2k^2+\omega_e^2)}\left(\frac{\xi}{\chi^2}E_y'\right)'\right), \tag{B 4b}$$

where ω_e is the electron plasma frequency discussed in appendix A, $\chi \equiv \gamma_0(\lambda+\mathrm{i}kV_0)$, $\xi \equiv \gamma_0(\lambda V_0/c^2+\mathrm{i}k)$, $P \equiv (qp)/(\varepsilon_0 fm)$ and primes indicate derivatives with respect to x.

Away from the discontinuity, V_0 is constant and pulls through the primes. Solving the resulting equations and assuming that perturbations vanish as x goes to plus or minus infinity, pressure satisfies

$$\left(\frac{\chi^2+\omega_e^2}{V_{te}^2}-\xi^2\right)P = P'' \rightarrow \tag{B 5}$$

$$P_a = P_a\mathrm{e}^{-xW_a} \tag{B 6a}$$

$$P_b = P_b\mathrm{e}^{xW_b} \quad \text{where } W_{a/b} \equiv \sqrt{\frac{\chi_{a/b}^2+\omega_e^2}{V_{te}^2}-\xi_{a/b}^2} \tag{B 6b}$$

and indices a and b indicate above and below the discontinuity, e.g. $\chi_a = \gamma_0(\lambda+\mathrm{i}kV_0)$, $\chi_b = \gamma_0(\lambda-\mathrm{i}kV_0)$. Similarly for E_y,

$$\left(\frac{\chi^2+\omega_e^2}{V_{te}^2}-\xi^2\right)(R^2E_y - E_y'') = (R^2E_y - E_y'')'' \rightarrow \tag{B 7}$$

$$E_{ya} = E_a\mathrm{e}^{-xR} - \frac{\xi_a}{\chi_a^2+\omega_e^2}P_a\mathrm{e}^{-xW_a}, \tag{B 8a}$$

$$E_{yb} = E_b\mathrm{e}^{xR} - \frac{\xi_b}{\chi_b^2+\omega_e^2}P_b\mathrm{e}^{xW_b} \quad \text{where } R = \sqrt{\frac{\lambda^2+c^2k^2+\omega_e^2}{c^2}}. \tag{B 8b}$$

https://doi.org/10.1017/S0022377816000180 Published online by Cambridge University Press

There are now four unknowns (E_{ya}, E_{yb}, P_a, P_b). To solve apply the boundary conditions ($P_a(0) = P_b(0)$ and $E_{ya}(0) = E_{yb}(0)$) and jump conditions (from integrating (B 4) across the discontinuity). The solution is

$$0 = R(\chi_a^2(\chi_b^2 + \omega_e^2) + \chi_b^2(\chi_a^2 + \omega_e^2))((\chi_a^2 + \omega_e^2)W_b + (\chi_b^2 + \omega_e^2)W_a) - \omega_e^2((\chi_a^2 + \omega_e^2)\xi_b - \xi_a(\chi_b^2 + \omega_e^2))^2. \tag{B 9}$$

Substituting in for χ and ξ and normalizing with

$$\frac{V_{te}}{c} \to V_{te}, \quad \frac{V_0}{c} \to V_0, \quad \frac{\gamma_0 \lambda}{\omega_e} \to \lambda, \quad \frac{\gamma_0 ck}{\omega_e} \to k \tag{B 10a–d}$$

results in (2.1).

REFERENCES

ALVES, E. P., GRISMAYER, T., MARTINS, S. F., FIUZA, F., FONSECA, R. A. & SILVA, L. O. 2012 Large-scale magnetic field generation via the kinetic Kelvin–Helmholtz instability in unmagnetized scenarios. *Astrophys. J.* **746** (2), L14.

ALVES, E. P., GRISMAYER, T., FONSECA, R. A. & SILVA, L. O. 2014 Electron-scale shear instabilities: magnetic field generation and particle acceleration in astrophysical jets. *New J. Phys.* **16**, 035007.

ALVES, E. P., GRISMAYER, T., FONSECA, R. A. & SILVA, L. O. 2015 Transverse electron-scale instability in relativistic shear flows. *Phys. Rev.* E **92**, 021101.

BISKAMP, D. 2003 *Magnetohydrodynamic Turbulence*. Cambridge University Press.

BRET, A., FIRPO, M.-C. & DEUTSCH, C. 2004 Collective electromagnetic modes for beam–plasma interaction in the whole K space. *Phys. Rev.* E **70**, 046401.

FIUZA, F. *et al.* 2012 Weibel-instability-mediated collisionless shocks in the laboratory with ultraintense lasers. *Phys. Rev. Lett.* **108**, 235004.

GREGORI, G. *et al.* 2012 Generation of scaled protogalactic seed magnetic fields in laser-produced shock waves. *Nature* **481**, 480–483.

GRISMAYER, T., ALVES, E. P., FONSECA, R. & SILVA, L. O. 2013 DC magnetic field generation in unmagnetized shear flows. *Phys. Rev. Lett.* **111**, 015005.

GRUZINOV, A. 2008 GRB: magnetic fields, cosmic rays, and emissions from first principles? arXiv:0803.1182.

GRUZINOV, A. & WAXMAN, E. 1999 Gamma-ray burst afterglow: polarization and analytic light curves. *Astrophys. J.* **511**, 852–861.

KULSRUD, R. M. & ZWEIBEL, E. G. 2008 On the origin of cosmic magnetic fields. *Rep. Prog. Phys.* **71**, 046901.

MAHAJAN, S. M. 2003 Temperature-transformed 'minimal coupling': magnetofluid unification. *Phys. Rev. Lett.* **90**, 035001.

MEDVEDEV, M. V. & LOEB, A. 1999 Generation of magnetic fields in the relativistic shock of gamma-ray burst sources. *Astrophys. J.* **526**, 697–706.

MILLER, E. & ROGERS, B. 2015 Magnetogenesis through convection in barotropic fluids. *Phys. Plasmas* **22**, 042104.

NISHIKAWA, K. I. *et al.* 2013 Magnetic field generation in a jet-sheath plasma via the kinetic Kelvin–Helmholtz instability. *Ann. Geophys.* **31**, 1535.

STOCKEM, A. *et al.* 2014 Exploring the nature of collisionless shocks under laboratory conditions. *Sci. Rep.* **4**, 3934.

SYNGE, J. L. 1957 *The Relativistic Gas*. Interscience Publishers.

WEIBEL, E. S. 1959 Spontaneously growing transverse waves in a plasma due to an anisotropic velocity distribution. *Phys. Rev. Lett.* **2**, 83.

https://doi.org/10.1017/S0022377816000180 Published online by Cambridge University Press